2021-03-23

The generalized Ekman model for the tropical cyclone boundary layer revisited: Addendum

Smith, Roger K.; Montgomery, Michael T.

Wiley

Smith, Roger K., and Michael T. Montgomery. "The generalized Ekman model for the tropical cyclone boundary layer revisited: Addendum." Quarterly Journal of the Royal Meteorological Society 147.736 (2021): 1471-1476.
http://hdl.handle.net/10945/69406

Received: 30 December 2020 | Revised: 27 February 2021 | Accepted: 28 February 2021 | Published on: 23 March 2021

DOI: 10.1002/qj.4012

Quarterly Journal of the Royal Meteorological Society RMetS

INVITED MANUSCRIPT

The generalized Ekman model for the tropical cyclone boundary layer revisited: Addendum

Roger K. Smith[1] | **Michael T. Montgomery**[2]

[1]Meteorological Institute, Ludwig-Maximilians University, Munich, Germany

[2]Department of Meteorology, Naval Postgraduate School, Monterey, California

Correspondence
R. K. Smith, Meteorological Institute, Ludwig-Maximilians University, Theresienstrasse 37, 80333 Munich, Germany.
Email: roger.smith@lmu.de

Abstract

Motivated by prior research examining the myth of inertial stability as a radial restoring force in the tropical cyclone boundary layer, we explore factors determining the vertical velocity at the top of the linear vortex boundary layer. Possible applications of these findings to mature tropical cyclone vortices are discussed briefly.

KEYWORDS

boundary layer, generalized Ekman balance, inertial stability, tropical cyclones

1 | INTRODUCTION

In a recent article Smith and Montgomery (2020), we revisited the linear boundary-layer approximation that expresses a generalized Ekman balance and used it to clarify a range of interpretations in the previous literature on the tropical cyclone boundary layer. Shortly after the article was published online, we discovered a plotting error in the vertical velocity, an error that spilled over into plots of estimates for the vertical and total advection terms in the nonlinear problem. While the changes in most of the figures were not large and have been published as a Correction (Smith and Montgomery, 2021), our discovery led us to explore in more detail the factors determining the vertical motion at the top of the linear boundary layer. In the present note, we present the new insights gained from the foregoing exploration. In view of recent work highlighting the utmost importance of the boundary-layer formulation in tropical cyclone forecast models (Zhang and Rogers, 2019; Zhang *et al.*, 2017; 2020), we hope that this extension of our study will be of value. While we are aware of the limitations of Ekman balance in the high wind region of a tropical cyclone boundary layer (Smith and Montgomery, 2020), we believe it is useful to explore the predictions of the model as a baseline for future analyses using nonlinear boundary-layer models.

2 | THE GENERALIZED EKMAN BOUNDARY LAYER

As shown by Smith and Montgomery (2020), the axisymmetric, tangential, radial, and vertical velocity components, $(u(r,z), v(r,z), w(r,z))$, for the steady generalized Ekman boundary layer on an f-plane, where f is the Coriolis parameter, assumed to be constant, are

$$v(r,z) = v_g(r)[1 + e^{-z/\delta}(a_1 \cos(z/\delta) + a_2 \sin(z/\delta))], \quad (1)$$

$$u(r,z) = -\chi v_g(r) e^{-z/\delta}(a_2 \cos(z/\delta) - a_1 \sin(z/\delta)), \quad (2)$$

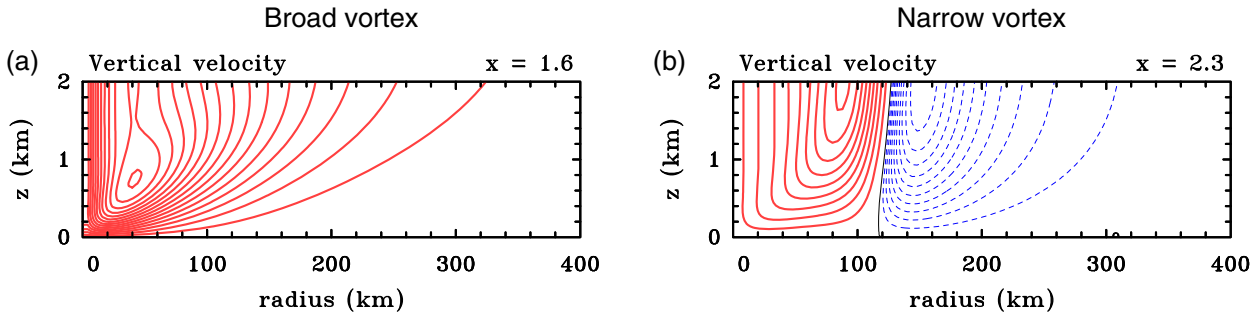

FIGURE 1 Isopleths of vertical velocity w in the r–z plane obtained from Equation 3 with the two tangential wind profiles shown in figure 1 of Smith and Montgomery (2020). (a) Broad gradient wind profile ($x = 1.6$), (b) narrow gradient wind profile ($x = 2.3$). Contour intervals: for $w > 0$, 0.02 m·s^{-1} for the broad profile or 0.05 m·s^{-1} for the narrow profile (red contours); for $w < 0$, 0.01 m·s^{-1} for the narrow profile (thin blue contours) [Colour figure can be viewed at wileyonlinelibrary.com]

$$w(r,z) = \frac{1}{r}\frac{\partial}{\partial r}\left[\frac{rKv_g}{\zeta_{ag}\delta}\left((a_2-a_1)\left\{1-e^{-z/\delta}\cos\frac{z}{\delta}\right\} + e^{-z/\delta}(a_1+a_2)\sin\frac{z}{\delta}\right)\right], \quad (3)$$

where r is the radius, z is the height, $v_g(r)$ is the gradient wind, $\delta = (2K/I)^{1/2}$ is the vertical scale for the boundary-layer depth, K is the local vertical turbulent diffusivity for horizontal momentum (assumed independent of height), ζ_{ag} is the absolute vorticity of the gradient wind, and a_1, a_2, and χ are known functions of radius that involve the surface drag coefficient, C_d.

In their figure 2, Smith and Montgomery (2020) showed solutions for the three velocity components for two radial profiles of gradient wind typical of tropical cyclones shown in their figure 1: a relatively broad profile and a relatively narrow profile.[1] The broad profile is consistent with the radial structure of mature tropical cyclones as observed by research aircraft (Mallen *et al.*, 2005), while the narrow profile is consistent with the structure of a rapidly developing storm in its early stages, in which the outer winds have not yet been appreciably amplified. The corrected radius–height cross-sections of vertical velocity are shown in Figure 1. While the structure of vertical velocity for the narrow profile is qualitatively and quantitatively similar to that in the original article, the structure for the broad profile is markedly different, with no region of subsidence. The fact that these structures would be predicted by the classical Ekman-layer solution led us to investigate further the factors determining the vertical velocity in the generalized Ekman solution.

[1]The formula for these profiles is $v_g(r) = v_1 s/(1+s^x)$, where $s = s_m r/r_m$, r is the radius, $r_m = 40$ km and s_m and v_1 are constants chosen to make $v = v_{gm}$, the maximum tangential wind speed, when $r = r_m$. The broad profile has $x = 1.6$ and the narrow profile $x = 2.3$.

3 | WHAT DETERMINES THE VERTICAL VELOCITY?

The formula for the vertical velocity (Equation 3) is sufficiently complex as it stands to obscure the main factors that determine the vertical velocity, and even the factors that determine the vertical velocity, $w(r,\infty)$, at the top of the boundary layer. The formula for $w(r,\infty)$ is a little simpler:

$$w(r,\infty) = \frac{1}{r}\frac{\partial}{\partial r}\left[\frac{rKv_g}{\zeta_{ag}\delta}(a_2-a_1)\right], \quad (4)$$

which may be expanded out to give

$$w(r,\infty) = \underbrace{\frac{K\zeta_g}{\zeta_{ag}\delta}(a_2-a_1)}_{w_1} + \underbrace{\frac{v_g}{\zeta_{ag}\delta}(a_2-a_1)\frac{\partial K}{\partial r}}_{w_2} \underbrace{-\frac{Kv_g}{\zeta_{ag}^2\delta}(a_2-a_1)\frac{\partial \zeta_{ag}}{\partial r}}_{w_3} + \underbrace{\frac{Kv_g}{\zeta_{ag}}\frac{d}{dr}\left(\frac{a_2-a_1}{\delta}\right)}_{w_4}, \quad (5)$$

where ζ_g is the relative vorticity of the gradient wind and $\zeta_{ag} = \zeta_g + f$. Here, for utmost generality, we have allowed the vertical turbulent diffusivity to be a function of r. The first term is familiar from Ekman theory itself, in which ζ_{ag} is approximated by f, K is assumed to be constant and a no slip boundary condition is assumed. In this case, $a_1 = -1$, $a_2 = 0$ and the terms w_2, w_3, and w_4 are all zero.

The second term on the right-hand side of Equation 5, w_2, is the contribution to $w(r,\infty)$ arising from the radial variation of turbulent diffusivity. This contribution is zero for the calculations shown in Smith and Montgomery (2020), because K was taken to be constant for simplicity. However, allowing K to vary radially might be quite important (see Section 4). The third term, w_3, is the contribution to $w(r,\infty)$ arising from the radial variation of

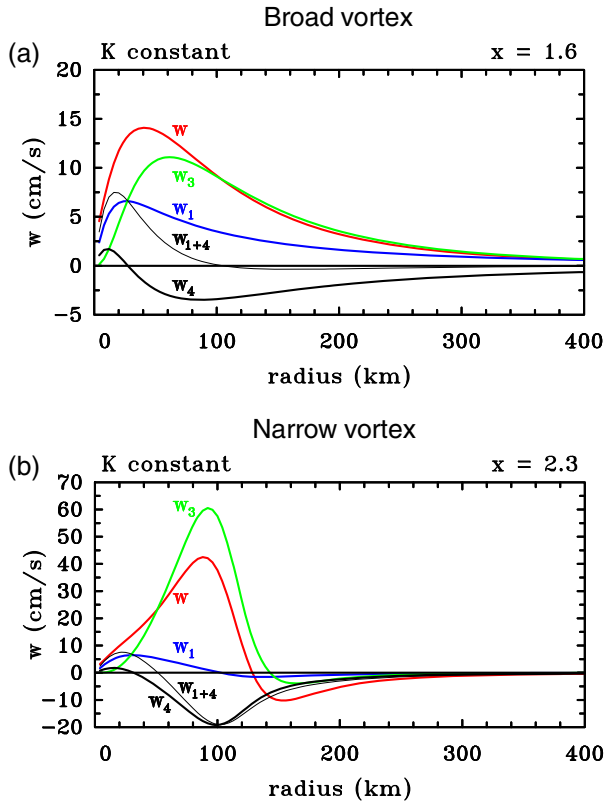

FIGURE 2 Radial profiles of the vertical velocity at the top of the boundary layer, $w(r,\infty)$ (labelled w), obtained from Equation 5 with the two tangential wind profiles shown in figure 1 of Smith and Montgomery (2020), together with the separate contributions from the terms w_1, w_3, and w_4. The values (a) $x=1.6$ and (b) $x=2.3$ refer to the broad and narrow gradient wind profiles, respectively. The thin black curves labelled $w_{1+4}=w_1+w_4$ are referred to in Section 5 [Colour figure can be viewed at wileyonlinelibrary.com]

relative vorticity of the gradient wind (note that, with f assumed constant, $\partial\zeta_{ag}/\partial r=\partial\zeta_g/\partial r$). The fourth term, w_4, contains the effects of radial changes in C_d through the dependence of a_1 and a_2 on C_d, which, in general depends on surface wind speed.[2] However, a_1 and a_2 depend on v_g, so that, even if C_d is taken to be constant, as in the calculations of Smith and Montgomery (2020), w_4 also depends on the radial gradient of v_g.

Since the gradient wind profile for the broad vortex used by Smith and Montgomery (2020) has positive relative vorticity ζ_g at all radii, Ekman theory would predict that $w(r,\infty)>0$ at all radii also. This observation raises the question as to whether w_1 is the dominant term in the calculation of $w(r,\infty)$ for the generalized Ekman calculation. To investigate this question, we have computed the separate contributions to $w(r,\infty)$ from the terms w_1, w_3, and w_4 in the calculations relating to Figure 1 (because K was assumed constant in these calculations, w_2 is zero). These, together with $w(r,\infty)$ itself, are shown in Figure 2.

It may be seen immediately that, for both narrow and broad radial profiles of gradient wind, the answer to the foregoing question is a resounding "no", except at large radii. In the case of the broad profile, w_3 and w_4 are opposite in sign at radii beyond about 30 km. At large radii, beyond about 300 km, they approximately cancel, whereupon $w(r,\infty)$ is approximated well by w_1. However, as the radius decreases, w_3 becomes larger in magnitude than w_4 and the sum w_3+w_4 makes a significant contribution to $w(r,\infty)$, comparable in magnitude to w_1. The upshot is that the maximum in $w(r,\infty)$ is about twice as large as that of w_1 and it occurs at a somewhat larger radius, close to the radius of maximum gradient wind (i.e., 40 km) rather than well inside it. Note that the radius of maximum w_1 occurs well inside the radius of maximum gradient wind. In contrast, for the narrow profile, w_3 and w_4 are both negative at radii beyond about 140 km and both are larger in magnitude than w_1. Moreover, for $r>140$ km, w_4 and w_3 are essentially comparable and thus w_3 does not dominate the expression for w.

It is worth noting that, for the same parameter values, the maximum vertical velocity is about four times as large for the narrow tangential wind profile as for the broad one.

4 | EFFECTS OF RADIALLY VARYING TURBULENT DIFFUSIVITY

At this stage, it is pertinent to ask how much the vertical velocity would be affected by variations in the turbulent diffusivity with radius. These effects would lead to a nonzero contribution from w_2 in Equation 5, as well as modifications to w_1, w_3, and w_4 through their dependence on K and δ, which depends also on K. While the only observational guidance that we are aware of to formulate such a variation is that of Zhang *et al.* (2011), numerical model simulations with a range of boundary-layer parameterizations do point to a substantial increase in K with wind speed (e.g., Smith and Thomsen, 2010; Zhang *et al.*, 2017, their figure 1; Zhang *et al.*, 2020, their figure 1). To illustrate the importance of such variations, we show in Figure 3 the vertical velocity at the top of the boundary layer and the contributions to it from the terms w_1-w_4 in two calculations where K increases linearly with decreasing radius. The slope is taken so that $K=10\,\mathrm{m^2\cdot s^{-1}}$ at radius 400 km and $50\,\mathrm{m^2\cdot s^{-1}}$ at radius 100 km. This postulated behavior is consistent with the observed dependence of K on wind speed shown in figure 10 of (Zhang *et al.*,

[2]The formulae for a_1 and a_2 are given in Equation 6 below. The dependence of a_1 and a_2 on C_d arises from the dependence of ν on C_d. Here ν is a local Reynolds number multiplied by the surface drag coefficient as defined below.

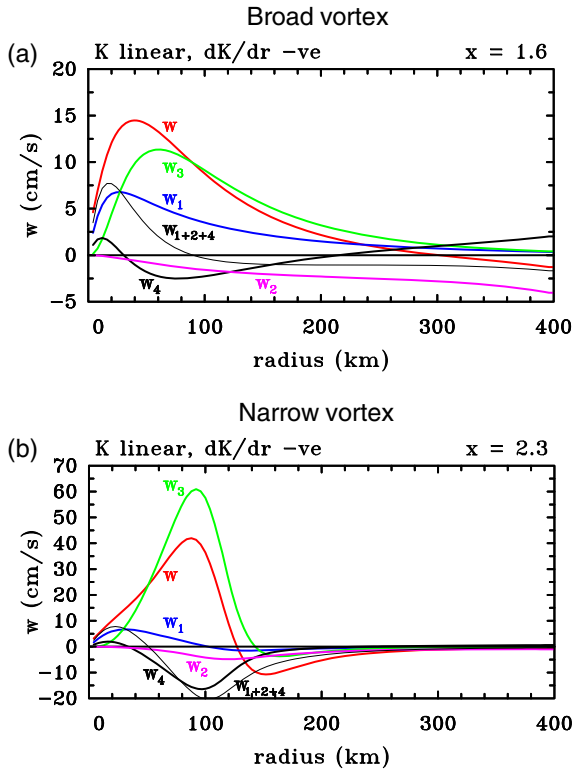

FIGURE 3 Radial profiles of the vertical velocity at the top of the boundary layer $w(r,\infty)$ (labelled w) obtained from Equation 5 with the two tangential wind profiles shown in figure 1 of Smith and Montgomery (2020), together with the separate contributions from the terms $w_1 - w_4$ in the calculations, with a linear increase of turbulent diffusivity with decreasing radius as described in the text. The values (a) $x = 1.6$ and (b) $x = 2.3$ refer to the broad and narrow gradient wind profiles, respectively. The thin black curves labelled $w_{1+2+4} = w_1 + w_2 + w_4$ are referred to in Section 5 [Colour figure can be viewed at wileyonlinelibrary.com]

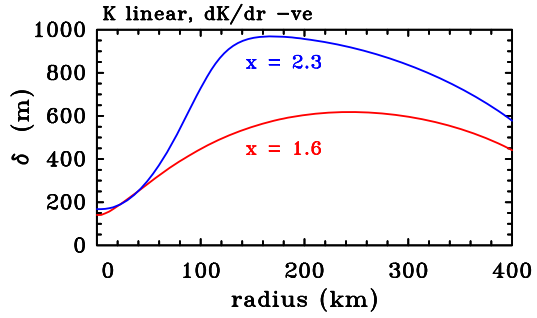

FIGURE 4 Radial profiles of the boundary-layer depth scale, $\delta(r)$ with the two tangential wind profiles shown in figure 1 of Smith and Montgomery (2020) and a linear increase of turbulent diffusivity with decreasing radius as described in the text. The values (a) $x = 1.6$ and (b) $x = 2.3$ refer to the broad and narrow gradient wind profiles, respectively. The sign "−ve" is to remind the reader that $dK/dr < 0$ [Colour figure can be viewed at wileyonlinelibrary.com]

2011). The two calculations relate to the broad and narrow vortices used earlier. The boundary-layer depth scale variations, $\delta(r)$, implied by the variation of K and ζ_{ag} are shown in Figure 4.

When K increases with decreasing radius (i.e., $dK/dr < 0$), so does the boundary-layer depth scale, δ, at least at large radii (Figure 4). Subsequently, as the rapid increase in ζ_{ag} in the denominator of the formula for δ begins to dominate the increase in K in the numerator, δ begins to decrease as r decreases. Since $a_1 < 0$ and $a_2 > 0$, all terms multiplying dK/dr in the expression for w_2 are positive, implying that $w_2 < 0$. The effect is particularly noticeable for the broad profile (Figure 3a), where it seen that w_2 is largest in magnitude at outer radii, but the large subsidence implied there is mitigated by the effect of w_4, which is now positive (recall that w_4 is mostly negative in the case of constant K: see Figure 3a). Nevertheless, the effect of increasing K with decreasing radius does lead to subsidence at large radii for the broad profile, contrary to the situation for constant K.

The contribution of w_2 to w is much smaller in the case of the narrow vortex (compare Figure 3b with Figure 3a). It is worth noting that, for each tangential wind profile, the maximum vertical velocity in the inner-core region is hardly affected by allowing the value of K to decrease with radius. In essence, this is because the generalized Ekman solution is a local one and the values of K near the maximum vertical velocity are similar.

5 | COMPARISON WITH PREVIOUS WORK

In a previous derivation, Kepert (2001) presented a formula for $w(r,\infty)$ that appears to have a rather different form from Equation 5. In our notation, this formula, his equation 28, can be written

$$w(r,\infty) = \frac{1}{r}\frac{\partial}{\partial r}\left[\frac{C_d r v_g}{\zeta_{ag}}(v_g + 2v'(0))\right]. \tag{6}$$

Kepert- remarked on the fact that this formula is nearly independent of the diffusivity K, stating that only the weak influence through $v'(0)$ remains. The same remark would not seem to be applicable to Equation 5, where K appears explicitly as well as implicitly through the dependence of δ and the coefficients a_1 and a_2 on K. However, using Equation 1 and the corrected expressions for the coefficients a_1 and a_2, that is,

$$a_1 = -\frac{\nu(\nu+1)}{2\nu^2+3\nu+2}, \quad a_2 = \frac{\nu}{2\nu^2+3\nu+2}, \tag{7}$$

it follows that

$$v_g + 2v'(0) = v_g(1 + 2a_1) = v_g\frac{a_2 - a_1}{\nu}. \quad (8)$$

Since $\nu = C_d v_g \delta / K$, it is easily verified that Equations 5 and 6 are identical. As shown in Section 3, there are several implicit dependences in the formula for $w(r, \infty)$ that complicate interpretations.

In a more recent article, Kepert (2013) expanded out his formula 6 to obtain, in our notation,

$$w(r,\infty) = -\frac{1}{\zeta_{ag}^2}\frac{\partial \zeta_{ag}}{\partial r} C_d v_g (v_g + 2v'(0)) + \frac{1}{r\zeta_{ag}}\frac{\partial}{\partial r}[rC_d v_g (v_g + 2v'(0))]. \quad (9)$$

Again, using Equation 7, it follows that the first term on the right-hand side of Equation 9 is w_3 in Equation 5, while the second term is simply the sum $w_1 + w_2 + w_4$, which is plotted as a thin black curve in Figures 2 and 3 (remember that $w_2 = 0$ in Figure 2). Kepert refers to the two terms on the right-hand side of Equation 9 as the "vorticity-gradient term" and "stress curl term", respectively. Although Kepert's decomposition of $w(r, \infty)$ is more compact than that in Equation 5, it does not lead to a simpler interpretation, because many effects are still implicit, including that involving the radial variation of K. In particular, for the broad and narrow profiles studied here, one cannot argue that either term in Equation 9 is everywhere dominant over the other. This is true for calculations with both constant K and variable K. Specifically, in the variable K case, which is arguably most relevant for realistic applications, the vorticity-gradient term fails to accurately represent the frictionally induced subsidence beyond a radius of 300 km in the broad vortex case and 125 km in the narrow case, where this subsidence represents a non-negligible sink to the boundary-layer energetics in transporting dry air into the boundary layer (see Ooyama, 1997, section 3.4).

6 | DISCUSSION AND CONCLUSIONS

We have examined the factors that determine the structure of azimuthally averaged vertical velocity at the top of a linearized Ekman boundary layer for two classes of tropical-cyclone-like tangential wind profiles.

In the first class, the wind profile is a "broad" profile and consistent with a modified Rankine vortex decaying approximately as 1/(radius)$^{0.6}$ outside the maximum wind region. This profile is consistent with the radial structure of mature tropical cyclones as observed by research aircraft. In this case, linear Ekman theory predicts a weak rising motion at all radii outside the radius of maximum tangential wind. This frictionally forced rising motion would tend to induce deep convective and rainband activity outside the main eyewall updraught, provided the thermodynamic and environmental conditions are favorable to support deep convective activity.

In the second class of vortex profiles, the tangential wind profile is relatively "narrow" and closer to a one-over-radius dependence. This second wind profile is consistent with the structure of a rapidly developing storm in its early stages, in which the outer winds have not yet been amplified appreciably. In this case, linear Ekman theory predicts weak, but persistent, subsidence into the frictional boundary layer that is associated with a slow radial acceleration of air parcels down the effective radial pressure gradient. Deep convection and spiral rainband activity would tend to be suppressed in this case and we expect the convective activity to be localized around the radius of maximum wind.

We showed that the vertical velocity at the top of the boundary layer can be written as the sum of four terms, including one that reduces to the classical Ekman formula in the Ekman limit, one characterizing the radial variation of turbulent eddy diffusivity, one characterizing the radial variation of absolute vorticity of the gradient wind, and one that has no simple physical interpretation. We showed that the term that reduces to the classical Ekman formula is not the dominant contribution to the vertical velocity in the vortex inner core for either the broad or narrow tangential wind profile, but it is the dominant contribution at large radii for both profiles. Significantly, the maximum vertical velocity is about four times as large for the narrow tangential wind profile as for the broad one. If the turbulent eddy diffusivity is allowed to decrease with increasing radius, the maximum vertical velocity in the inner-core region for each tangential wind profile is hardly affected by allowing the value of K to decrease with radius: the largest effect is at large radii.

Finally, we show that the decomposition of the vertical velocity at the top of the boundary layer is not unique and compare our decomposition with an alternative one that has been used in the literature.

ACKNOWLEDGEMENTS

MTM acknowledges the support of NSF grants AGS-1313948 and IAA-1656075, ONR grant N0001417WX 00336, and the U.S. Naval Postgraduate School. The views expressed herein are those of the authors and do not represent sponsoring agencies or institutions. Open access funding enabled and organized by Projekt DEAL.

ORCID

Roger K. Smith https://orcid.org/0000-0002-3668-1608
Michael T. Montgomery https://orcid.org/0000-0001-5383-4648

REFERENCES

Kepert, J.D. (2001) The dynamics of boundary layer jets within the tropical cyclone core. Part I: linear theory. *Journal of the Atmospheric Sciences*, 58, 2469–2484.

Kepert, J.D. (2013) How does the boundary layer contribute to eyewall replacement cycles in axisymmetric tropical cyclones?. *Journal of the Atmospheric Sciences*, 70, 2808–2830.

Mallen, K.J., Montgomery, M.T. and Wang, B. (2005) Reexamining the near-core radial structure of the tropical cyclone primary circulation: implications for vortex resiliency. *Journal of the Atmospheric Sciences*, 62, 408–425.

Ooyama, K.V. (1997). Footnotes to 'Conceptual Evolution'. In:, *Extended Abstracts, 22nd Conference on Hurricanes and Tropical Meteorology*. Boston, MA: American Meteorological Society.

Smith, R.K. and Montgomery, M.T. (2020) The generalized Ekman model for the tropical cyclone boundary layer revisited: the myth of inertial stability as a restoring force. *Quarterly Journal of the Royal Meteorological Society*, 146, 3435–3449.

Smith, R.K. and Montgomery, M.T. (2021) Correction to: The generalized Ekman model for the tropical cyclone boundary layer revisited. *Quarterly Journal of the Royal Meteorological Society*, 147. https://doi.org/10.1002/qj.3999.

Smith, R.K. and Thomsen, G.L. (2010) Dependence of tropical-cyclone intensification on the boundary layer representation in a numerical model. *Quarterly Journal of the Royal Meteorological Society*, 136, 1671–1685.

Zhang, J.A., Kalina, E.A., Biswas, M.K., Rogers, R.F., Zhu, P. and Marks, F. (2020) A review and evaluation of planetary boundary-layer parameterizations in Hurricane Weather Research and Forecasting model using idealized simulations and observations. *Atmosphere*, 11, 1091.

Zhang, J.A., Marks, F.D., Montgomery, M.T. and Lorsolo, S. (2011) An estimation of turbulent characteristics in the low-level region of intense Hurricanes Allen (1980) and Hugo (1989). *Monthly Weather Review*, 139, 1447–1462.

Zhang, J.A. and Rogers, R.F. (2019) Effects of parameterized boundary layer structure on hurricane rapid intensification in shear. *Monthly Weather Review*, 147, 853–871.

Zhang, J.A., Rogers, R.F. and Tallapragada, V. (2017) Impact of parameterized boundary layer structure on tropical cyclone rapid intensification forecasts in HWRF. *Monthly Weather Review*, 145, 1413–1426.

How to cite this article: Smith RK, Montgomery MT. The generalized Ekman model for the tropical cyclone boundary layer revisited: Addendum. *QJR Meteorol. Soc.* 2021;147:1471–1476. https://doi.org/10.1002/qj.4012